3-D bioprinted human-derived skin organoids accelerate full-thickness skin defects repair

Tao Zhang [a,b,1], Shihao Sheng [a,1], Weihuang Cai [c,1], Huijian Yang [d,1], Jiameng Li [b], Luyu Niu [b], Wanzhuo Chen [b], Xiuyuan Zhang [b], Qirong Zhou [b], Chuang Gao [c], Zuhao Li [a,e,f,g], Yuanwei Zhang [a,e,f,g], Guangchao Wang [a,f,g], Hao Shen [a,f,g], Hao Zhang [a,e,f,g], Yan Hu [a,f,g], Zhifeng Yin [e,h], Xiao Chen [a,f,g,****], Yuanyuan Liu [c,i,***], Jin Cui [b,e,**], Jiacan Su [a,e,j,k,*]

[a] Department of Orthopedics, Xinhua Hospital, Shanghai Jiao Tong University School of Medicine, Shanghai, 200433, China
[b] Department of Orthopedics, First Affiliated Hospital, Naval Medical University, Shanghai, 200433, China
[c] School of Mechatronic Engineering and Automation, Shanghai University, Shanghai, 200444, China
[d] Department of Laboratory Medicine, Shanghai Zhongye Hospital, Shanghai, 200941, China
[e] Institute of Translational Medicine, Shanghai University, Shanghai, 200444, China
[f] Trauma Orthopedics Center, Xinhua Hospital Affiliated to Shanghai Jiao Tong University School of Medicine, Shanghai, 200092, China
[g] Institute of Musculoskeletal Injury and Translational Medicine of Organoids, Xinhua Hospital Affiliated to Shanghai Jiao Tong University School of Medicine, Shanghai, 200092, China
[h] Department of Orthopedics, Shanghai Zhongye Hospital, Shanghai, 200941, China
[i] Wenzhou Institute of Shanghai University, Wenzhou, 325000, China
[j] Institute of Biomedicine, Shanghai University, Shanghai, 200444, China
[k] National Center for Translational Medicine (Shanghai), SHU Branch, Shanghai University, Shanghai, 200444, China

ARTICLE INFO

ABSTRACT

The healing of large skin defects remains a significant challenge in clinical settings. The lack of epidermal sources, such as autologous skin grafting, limits full-thickness skin defect repair and leads to excessive scar formation. Skin organoids have the potential to generate a complete skin layer, supporting in-situ skin regeneration in the defect area. In this study, skin organoid spheres, created with human keratinocytes, fibroblasts, and endothelial cells, showed a specific structure with a stromal core surrounded by surface keratinocytes. We selected an appropriate bioink and innovatively combined an extrusion-based bioprinting technique with dual-photo source cross-linking technology to ensure the overall mechanical properties of the 3D bioprinted skin organoid. Moreover, the 3D bioprinted skin organoid was customized to match the size and shape of the wound site, facilitating convenient implantation. When applied to full-thickness skin defects in immunodeficient mice, the 3D bioprinted human-derived skin organoid significantly accelerated wound healing through in-situ regeneration, epithelialization, vascularization, and inhibition of excessive inflammation. The combination of skin organoid and 3D bioprinting technology can overcome the limitations of current skin substitutes, offering a novel treatment strategy to address large-area skin defects.

1. Introduction

Wound healing is an intricate and dynamic process involving the participation of various cells and cytokines across four overlapping phases: hemostasis, inflammation, proliferation, and tissue remodeling [1–4]. Wounds of varying etiologies burden the healthcare system [5], with an estimated 100 million people globally suffering from acute or chronic wounds annually. The worldwide wound care market, estimated to be worth close to 20 billion in recent years, is forecasted to exceed 30.1 billion by the year 2030 [6,7]. In Northern China, the total cost of treating wounds in hospitals increased from 1.23 % in 2014 to 3.18 % in 2017 of total healthcare expenditures for each respective year [8]. The growing number of surgical cases, rising combat burns, and surge in traffic accidents worldwide have motivated the urgent need for advanced wound care products.

Unfortunately, despite numerous treatments available for wound healing, including various wound dressings, negative pressure wound therapy, hyperbaric oxygen therapy, and autologous skin flap grafts, their clinical efficacy remains unsatisfactory for massive skin defects [2, 9]. Skin organoids can address the extraordinary challenge of skin transplantation by providing an alternative for infertile wounds where peri-wound epidermal cells are inadequate to migrate and cover the entire wound area. These organoids contain the fundamental cells and biological construction of skin layers.

The capacity of skin organoids to develop integrated skin structures is incalculable. In 2020, Jiyoon et al. [10] engineered an organoid culture system capable of generating intricate skin constructs from human pluripotent stem cells in vitro. These constructs consist of a stratified epidermis, a dermis enriched with adipose tissue, and pigmented hair follicles integrated with sebaceous glands, which further develop into planar hair-bearing skin upon transplantation onto nude mice. The construction of organoids facilitates an intricate exploration into the nuances of intercellular communication, the spectrum of cellular heterogeneity, the regulation of tissue-specific gene and protein expressions, alongside the dynamics of metabolic activities [1]. This sophisticated model emulates the extracellular microenvironment intrinsic to living organisms, providing a platform for comprehensive biological inquiry [11,12,13].

Bio-engineered skin substitutes based on skin organoids can be applied to acute massive skin defects to address the shortage of skin regeneration and adverse wound substrates. Given the ethical concerns and the uncontrolled proliferation and differentiation attributes associated with embryonic stem cells (ESCs) and induced pluripotent stem cells (iPSCs), adult stem cells (ASCs) emerge as a promising alternative. ASCs, defined as tissue-specific stem cells, exhibit a propensity for tissue-restricted differentiation, thereby offering a more controlled and targeted approach [14,15]. Although they do not exhibit the broader pluripotency characteristic of ESCs and iPSCs, these cells possess multipotency, enabling them to differentiate into multiple cell types within their tissue of origin [16,17]. Based on cell accessibility and culture manufacturing, we utilized three types of skin layer cells to produce spherical skin organoids containing keratinocytes, fibroblasts, and vascular endothelial cells, demonstrating the basic skin structure in the epidermis, dermis, and neo-vessels. ASC-derived skin organoids have enormous application prospects.

However, there is an overwhelming demand for substrate support because scattered spherical skin organoids should not be implanted directly in practical application scenarios [18]. Three-dimensional (3D) bioprinting represents a sophisticated biofabrication methodology, meticulously depositing bioinks in accordance with preconceived designs to engineer tissues and organs that exhibit architectures closely emulating native biological structures [19–22]. Recent research has shown significant advancements in 3D bioprinting organoids, although bioprinting approaches have been predominantly used for bioprinting cells encapsulated in hydrogels [23]. Furthermore, three-dimensional (3D) bioprinting affords precise positioning of spherical organoids or cellular aggregates, thereby offering superior spatial regulation. This technique facilitates the direct amalgamation of these structures, paving the way for the formation of large-scale, functional tissues with enhanced structural integrity and physiological relevance in vitro [24, 25].

To adapt to the wound microenvironment, as shown in Fig. 1, we proposed a composite preparation process for 3D bioprinting skin organoids. The core idea of this method is to achieve effective embedding and assembly of spherical skin organoid hydrogels based on extrusion bioprinting technology under the action of a temperature field and a step-by-step photo-cross-linking composite molding method. First, spherical skin organoids were 3D printed by extrusion bioprinting and temperature-derived pre-crosslinking. Subsequently, to ensure the overall mechanical properties of the 3D bioprinted skin organoids, a photo-cross-linking process based on dual photo sources was innovatively proposed. This process ensures the mechanical properties of hydrogels. At the same time, the cross-linking process can reduce photo damage to cells by reducing the illumination time, providing a new solution to the problem of wound repair.

In our investigation, we utilized adult stem cells to produce spherical skin organoids, then combined them with 3D bioprinting to simulate a more authentic skin architecture. Biological complexes corroborated the regenerative capacity of 3D bioprinted skin organoids, underscoring their efficacy in accelerating wound closure in situ, fostering the maturation of an epidermal stratum mirroring native skin architecture, augmenting collagen synthesis, and stimulating neovascularization. Ultimately, through the application of RNA sequencing, we substantiated the role of 3D bioprinted skin organoids with a three-dimensional bionic structure in massive wound healing. This brings organoid research a step closer to translational clinical applications and provides more innovative insights into regenerative medicine.

2. Materials and methods

2.1. Materials

Human keratinocytes (HaCaT), human dermal fibroblasts, and human umbilical vein endothelial cell lines were sourced from Shanghai Sebachem Biotechnology Co. Dulbecco's modified Eagle's medium (DMEM), fetal bovine serum (FBS), streptomycin-penicillin solution, and 0.25 % trypsin were supplied by Thermo Fisher Scientific. Human Platelet Lysate (HPL) was obtained from Sexton Biotechnologies. K1, K10, K14, human VIM, human CD31, COL I, and COL III antibodies were purchased from Sevier Biotechnology Co.LTD. Gelatin methacrylate (GelMA) and lithium phenyl-2,4,6-trimethylbenzoylphosphinate (LAP) were procured from Yongqinquan Intelligent Equipment Co., Ltd, Suzhou, China.

2.2. Cells culture and experimental animals' welfare

All cell lines were maintained in Dulbecco's Modified Eagle Medium (DMEM; Gibco, catalog number 10567014) enriched with 10 % fetal bovine serum (FBS; Gibco, catalog number 10099141C) and 1 % antibiotic solution of streptomycin-penicillin (Gibco, catalog number 15140122). Cultivation occurred within a humidified incubator, set at 37 °C and supplied with 5 % CO_2. The culture medium underwent replenishment every alternate day. Upon reaching approximately 90 % confluency, cells were subcultured, with those from passages 4 through 7 deemed suitable for the construction of skin organoids. All immunodeficient BALB/c female mice, aged 6 weeks and weighing between 20 and 25 g, were sourced from Beijing Viton Lihua Laboratory Animal Technology Co., Ltd. The experimental animals were housed in an SPF-grade animal laboratory facility and acclimatized to the environment for one week prior to surgical procedures. Animal management procedures were approved by the Animal Ethics Committee of the First Affiliated Hospital of Naval Medical University (CHECAE2022009) under the
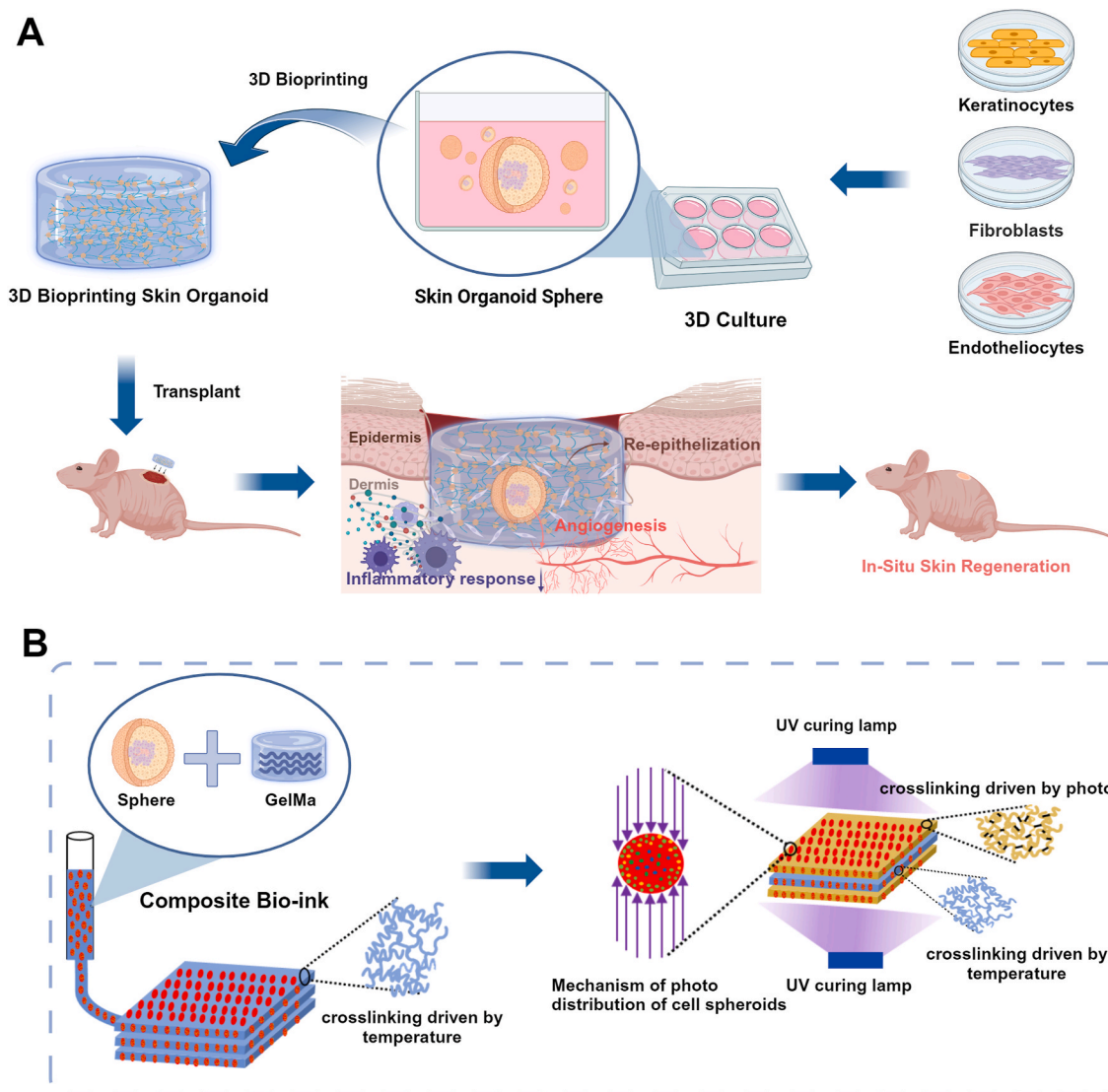
Fig. 1. The schematic diagram illustrates the preparation of 3D bioprinting skin organoid was developed from three adult stem cells for the restoration of large skin defects in situ and improved healing quality.

guideline.

2.3. Synthesis and formation of floating sphere skin organoid

Single-cell suspensions of keratinocytes, fibroblasts, and vascular endothelial cells were prepared at a ratio of 2:1:1 to generate sphere skin organoids. Briefly, 4 x 105 cells per cm^2 were seeded as single cells followed by self-assembly using ultra-low adsorbent material (Corning, 3471) for 24 h. The cells were exposed to DMEM fortified with 10 % HPL (Sexton, PL-NH-100) alongside a 1 % antibiotic solution of streptomycin-penicillin and the culture medium was replenished on alternate days. Microscopic analysis was performed 5 days after seeding (see image acquisition).

2.4. Physicochemical properties and biocompatibility of hydrogels

2.4.1. Swelling properties

Immediately freeze the printed samples at −80 °C. Subsequently, remove the moisture from the samples using a freeze dryer and measure the hydrogel mass (denoted as W0). Immerse the samples in PBS at 37 °C to determine the swelling ratio (SR). At various time points (1 h, 2 h, 4 h, 6 h, 24 h), retrieve the samples, dry the surface moisture with filter paper, and measure the sample mass (denoted as Wt). Finally, calculate the hydrogel SR using the following formula [26]:

$$SR = \frac{W_t - W_0}{W_0}$$

2.4.2. Rheological properties

The rheological properties of hydrogels were tested using a rheometer. The ambient temperature was set to 22 °C, and the shear rate variation range was set to 0.1–100 s-1. The viscosity is a determining factor for evaluating the rheological properties of hydrogels, which influences their printability.

2.4.3. Biocompatibility

The biocompatibility of the hydrogel was verified using three different skin cell types. Live/dead staining was used to label live and dead cells. According to the instructions (Solarbio), calcein-AM and propidium iodide (PI) were dissolved in PBS to prepare the experimental solution. Cell proliferation was detected using a cell counting kit-8 (CCK-8, Dojindo). The test mixture was prepared at a volume ratio of CCK-8 reagent: DMEM solution of 10:100 (v/v).

2.4.4. Printability and optimization of printing process parameters

The printability of the hydrogel was demonstrated by printing different shapes (polylines and spirals). To determine the main printing process parameters, the effects of different print speeds and extrusion speeds on hydrogel printing quality were studied.

2.5. 3D bioprinting skin organoid

Dissolve 0.2 g GelMA powder in 1 ml PBS, then add 1 mL LAP solution, and mix thoroughly at 40 °C to prepare bioink with concentrations of 10 % GelMA and 0.25 % LAP. Take 1.5 ml of biological ink and filter it using a 0.22 μm sterile filter. Then mix it thoroughly with the number of spherical skin organoids cultured in a 6-well plate, and finally load it into a 3 cc dispensing syringe. The size of the 3D bioprinting skin organoid is designed to be a cylindrical structure with a diameter of 10 mm and a thickness of 1 mm. The printer is based on pneumatic extrusion and uses a 22 g conical nozzle, the print speed and extrusion speed of printer are 1 mm/s and 1.5 mm^3/s (Axolotl Biosystems, Axo A3, AxoSuite 1.4.9) . Place the printed sample between two UV curing lamps. After exposing the front side for 10 s, expose the back side for another 10 s(UV lamp: EFL-LS-1601-405, 405 nm, 25mw/cm^2).

2.6. Animal experiments

Adult female BALB/c mice (8 weeks, 20.0 ± 5.0 g, n = 18) were employed to develop in vivo full-thickness wound healing paradigm. Each subject was rendered unconscious utilizing isoflurane anesthesia. A full-thickness, circular incision with a 10-mm diameter was meticulously excised from the dorsal epidermis of each animal to simulate a wound site. Hydrogels were fabricated with a diameter congruent to the wound size and the same storage modulus as described above. The mice were divided into three groups: Gel group (hydrogel implantation only), Gel + Susp group (implanted with cell suspension) and printed organoid group (implanted with 3D bioprinted skin organoid). After hydrogel implantation, all mice were fitted with anti-shrinkage rings to reduce autologous skin contraction on wound closure, and dressings were changed every 2 days. Wound images were captured using a digital camera, and wound closure area was analyzed using ImageJ software. All mice were maintained on a standard rodent diet to ensure consistent nutritional support throughout the study period. The mice were executed via CO_2 suffocation after 16 days, and the excised skin specimens were encapsulated within paraffin blocks for histological analysis.

2.7. Histology of FSOs and wound sections

Hematoxylin and eosin (H&E) as well as Masson's trichrome staining were conducted following established protocols. For H&E staining, rehydrated samples underwent hematoxylin treatment for 2 min and eosin treatment for 6 min at room temperature. Subsequently, the slides were dehydrated, mounted, and examined using optical microscopy.

Masson's trichrome staining was carried out in accordance with the manufacturer's instructions (Solarbio, G1340). In brief, the samples were sequentially stained with Weigert's iron hematoxylin solution, Biebrich scarlet acid fuchsin solution, and aniline blue solution. Subsequently, the stained samples were mounted for subsequent analysis.

2.8. Immunofluorescence staining and immunohistochemical staining of 3D bioprinting skin organoid and wound tissue

For immunofluorescence (IF) staining, Specimens were immobilized and subsequently incubated overnight at 4 °C with anti-VIM or anti-CD31 antibody solution (1:100 in blocking buffer; 5 % FBS and 0.1 % Tween-20 in PBS). The samples were then exposed to a biotin-conjugated anti-mouse IgG secondary antibody (1:100 in blocking buffer) and accompanied by a FITC-conjugated streptavidin tertiary antibody, similarly, diluted for a duration of 2 h at 37 °C. Post-

processing, the specimens were affixed and visualized under a fluorescent microscope to capture the resultant images. immunofluorescence (IF) staining of cytokeratins (K1, K10, K14), a primary antibody specific to these proteins was utilized, diluted at a ratio of 1:200 in the blocking buffer.

Immunohistochemical (IHC) staining was executed adhering to a standardized protocol up until the stage of primary antibody application, deploying anti-COL I and anti-COL III antibodies (1:200 in blocking buffer). Subsequently, the specimens underwent exposure to anti-rabbit IgG HRP-conjugated secondary antibody (1:500 in blocking buffer) for 2 h, followed by incubation with hematoxylin solution for a span of 2 min at ambient temperature. Conclusively, the samples were immersed in DAB substrate solution for a period of 10 min at room temperature to achieve the final chromogenic reaction.

2.9. RNA sequencing

At 16 days post-modeling, tissue samples from the wound areas of the three groups of mice were harvested following an identical protocol. The skin tissues were placed into cryovials, labeled according to their respective groups, snap-frozen in liquid nitrogen for 2 min, and subsequently stored at −80 °C until required for sequencing. For transcriptome sequencing and analysis, the samples were submitted to Shanghai OE Biotech Co., Ltd.

2.10. Data analysis

The results are articulated as the mean ± standard deviation (SD). Statistical assessments were executed utilizing IBM SPSS Statistics 20.0, complemented by graphical representation in Origin software. A one-way Analysis of Variance (ANOVA) was employed to ascertain statistical significance. A p-value threshold below 0.05 was deemed indicative of statistical significance. P values are denoted as: *$p < 0.05$, **$p < 0.01$, ***$p < 0.001$, ****$p < 0.0001$.

3. Results and discussion

3.1. Self-assembly of keratinocytes, fibroblasts and endothelial cells generated sphere skin organoid

Although skin organoids are not genuinely human skin, they can simulate the structure and function of human skin, such as the epidermis and dermis, and are not a mere aggregation of cells. Based on previous studies, progenitor cells isolated from various organs can self-assemble into spheroids when cultured in an ultralow attachment environment [12]. We created spherical skin organoids using three main components of skin. As shown in Fig. 2A, sphere skin organoids were constructed by the aggregation of human-derived keratinocytes, fibroblasts, and endothelial cells, accompanied by scattered cells distributed in the surrounding area after mixing the single-cell suspensions in a 2:1:1 proportion for one day. The spheroids gradually augmented as the culture prolonged, becoming larger and more spherical in shape. We observed that the cell clusters were tightly structured, and the stratification was in homogeneous rows, which is an integral morphology of sphere skin organoids, as demonstrated by H&E staining in Fig. 2B. It is evident that the pattern of cell arrangement is organized rather than disordered.

Sphere skin organoids were encapsulated by multi-layered epidermal cells, as shown in Fig. 2E. Peripheral keratinocytes were highly characterized by the expression of keratin 1/10/14, and Ki-67-positive cells were mainly located at the surface of the spheroid, suggesting that keratinocytes maintained an aggressive proliferative activity (Fig. 2C). The core of the spheroids consisted of dermal fibroblasts and vascular endothelial cells, which was coherent with the immunofluorescence labeling. VIM was expressed in the center of the sphere organoids as a specific marker for mesenchymal tissues derived from mesodermal
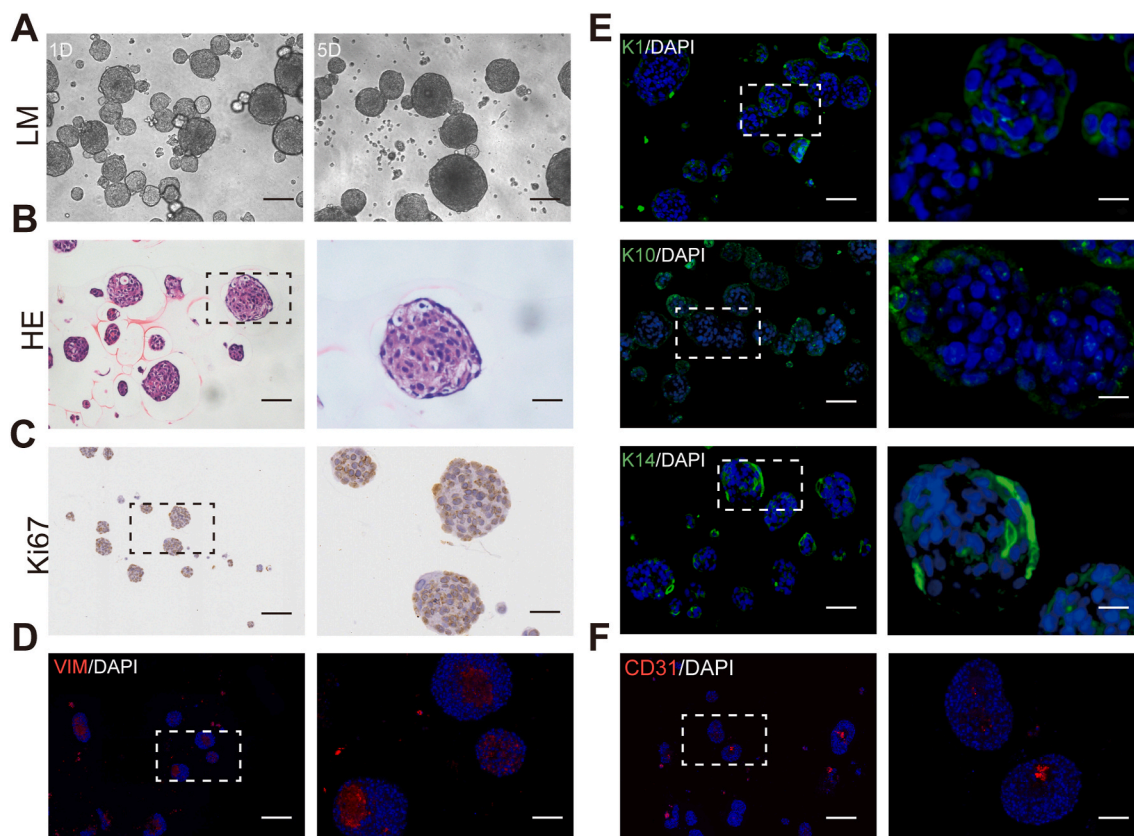
Fig. 2. The preparation and characterization of self-assembly sphere skin organoids. (A) Microscopic morphology of sphere skin organoids at day1 and day5. Scale bar, 75 μm (B to F) Histology of cross-sectioned organoids harvested at day 7. (B) Hematoxylin/eosin staining illustrated FSO organization. Scale bars, 100 μm and 50 μm. (C) Anti-Ki67 staining indicating cell proliferation within sphere skin organoids. Scale bars, 150 μm and 50 μm. Immunofluorescence staining results of anti-human vimentin (VIM, red, D), anti-human keratin 10/1/14 (K10, K1, and K14, green, E) and anti-human CD31 (red, F) confirmed cell organization into dermal core structures (VIM + CD31) and epidermal layered arrangement (K14). Scale bars, 100 μm and 25 μm. DAPI + nuclei in blue. (B–F) Frames indicating area shown in higher magnification at the right next to overview pictures.

origins (Fig. 2D) and was interspersed with early vasculogenesis (Fig. 2F). In conclusion, we successfully constructed sphere skin organoids in vitro with fibroblasts and vascular endothelial cells as the dermal core, peripherally wrapped by keratinocytes, which is potentially capable of developing into complete skin to replace massive skin defects.

3.2. Physicochemical properties and biocompatibility of hydrogels

Swelling performance is a commonly used indicator to evaluate the ability of hydrogels to absorb liquids. Hydrogels with good liquid absorption capabilities are conducive to the exchange of substances within the three-dimensional structure. As shown in Fig. 3A, the swelling ratio of different proportions of hydrogels was negatively correlated with concentration. The hydrogel swelling curves of the 5 % and 10 % GelMA groups showed similar trends, exhibiting rapid liquid absorption capacity in 0–2 h. As time increased, the swelling capacity changed gradually. The absorption of the 15 % GelMA hydrogel showed a slow increase throughout the process. The swelling ratios of different hydrogels at 24 h proved the excellent swelling capabilities of 5 % and 10 % GelMA hydrogels.

The test results of the rheological properties are shown in Fig. 3B. The viscosity ranges of 5 %, 10 %, and 15 % GelMA are 0.67–39.02 Pa s, 5.15–4343 Pa s, and 0.71–16780 Pa s, respectively. As the shear rate of each hydrogel group increases, the viscosity gradually decreases, showing typical shear-thinning characteristics. Hydrogels with shear-thinning properties can become smooth during bioprinting, making it easier to print tissues/organs with higher precision. The ideal bioink for extrusion-based bioprinting should flow easily when shear stress is applied and quickly stabilize to form a solid hydrogel after extrusion [27]. Moreover, it should be ensured that the sphere skin organoids are subject to small shear forces during the printing process. Considering the swelling and rheological properties, 10 % GelMA was used as the hydrogel concentration in the following studies.

HaCaT cells cultured in hydrogel-free well plates can attach normally to the surface (Fig. 3C). However, HaCaT cells seeded in well plates containing 10 % GelMA hydrogel tended to grow in clusters. After replacing the culture medium, almost no cells were found on the gel surface, indicating that HaCaT did not adhere to the hydrogel surface normally. Previous studies have shown that this phenomenon is related to the mechanical properties of the hydrogel, and higher concentrations of GelMA can promote the adhesion and proliferation of HaCaT [28,29].

Cell viability and proliferation tests of human skin fibroblasts (HSF) and human umbilical vein endothelial cells (HUVEC) were performed on days 1, 2, and 4 after culture, as shown in Fig. 3D. HSF exhibited high viability during culture, with only a few dead cells found. After 1 day of culture, there was no significant difference in HSF morphology. However, on the second and fourth days of culture, the cell morphology began to transform into an elongated spindle shape. On the fourth day, the cells grew and stretched significantly, and cell-cell contacts were observed. The CCK-8 results of HSF verified that as the culture time increased, HSF proliferation also increased, with significant statistical differences in cell proliferation at different culture times ($p < 0.01$). Most HUVEC showed green fluorescence at different culture times, indicating a high cell survival rate. HUVEC morphology also gradually changed during culture, although the rate of change was not as fast as
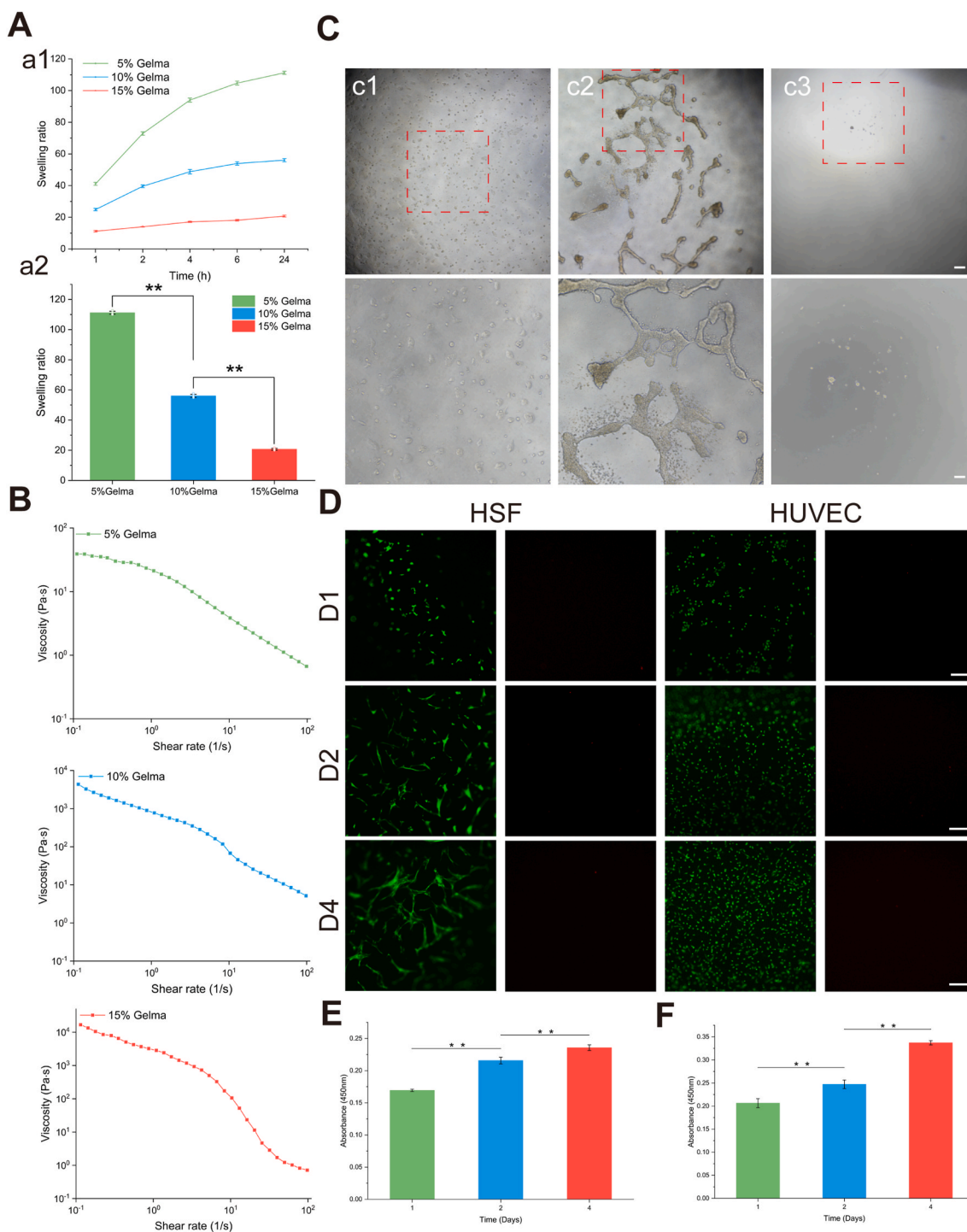
Fig. 3. Physicochemical properties and biocompatibility of hydrogels. (A)Swelling properties of GelMA with different ratios. a) Swelling rate of hydrogels as a function of time. b) Swelling ratios of different hydrogels at 24 h. (B)The curves of viscosity changes with shear rate of 5 % GelMA, 10 % GelMA, 15 % GelMA, respectively. Scale bar = 500 μm. (C)Growth status of HaCaT on the hydrogel surface. c1)-c3) show low magnification images of the cells in the well plate without hydrogel, in the well plate with hydrogel, and in the well plate with hydrogel (after changing the medium) after 1 day of culture, and high-magnification images. (D) Growth status of HSF and HUVEC on the hydrogel surface. Scale bar = 200 μm. (E) and(F) show the CCK-8 results of HSF and HUVEC.

that of HSF. In addition, HUVEC also showed strong proliferation ability on the hydrogel surface (Fig. 3E and F). The biological behavior of three types of skin cells on the hydrogel demonstrates that the ability of different skin cells to perceive the hydrogel varies.

To verify the printability of the bioink mentioned in section 2.5, the effect of different printing speeds on bioink printing quality was studied, keeping other conditions unchanged. The results are shown in Fig. 4A. As shown in the supplementary documents, when other parameters are

kept constant, as the extrusion speed increases, the size and shape of the fiber filaments gradually become uniform. It can also be concluded that 1.2–1.5 mm3/s is the optimal parameter for extrusion speed.

Further, the printing parameters were kept constant, and the effect of single and dual light source crosslinking on cell survival was investigated. The ratio of cell spheres to bioink was as described in section 2.5. The cell sphere-laden hydrogel samples were irradiated by a single-photo source for 40 s and a dual-photo source for 10 s, respectively, to
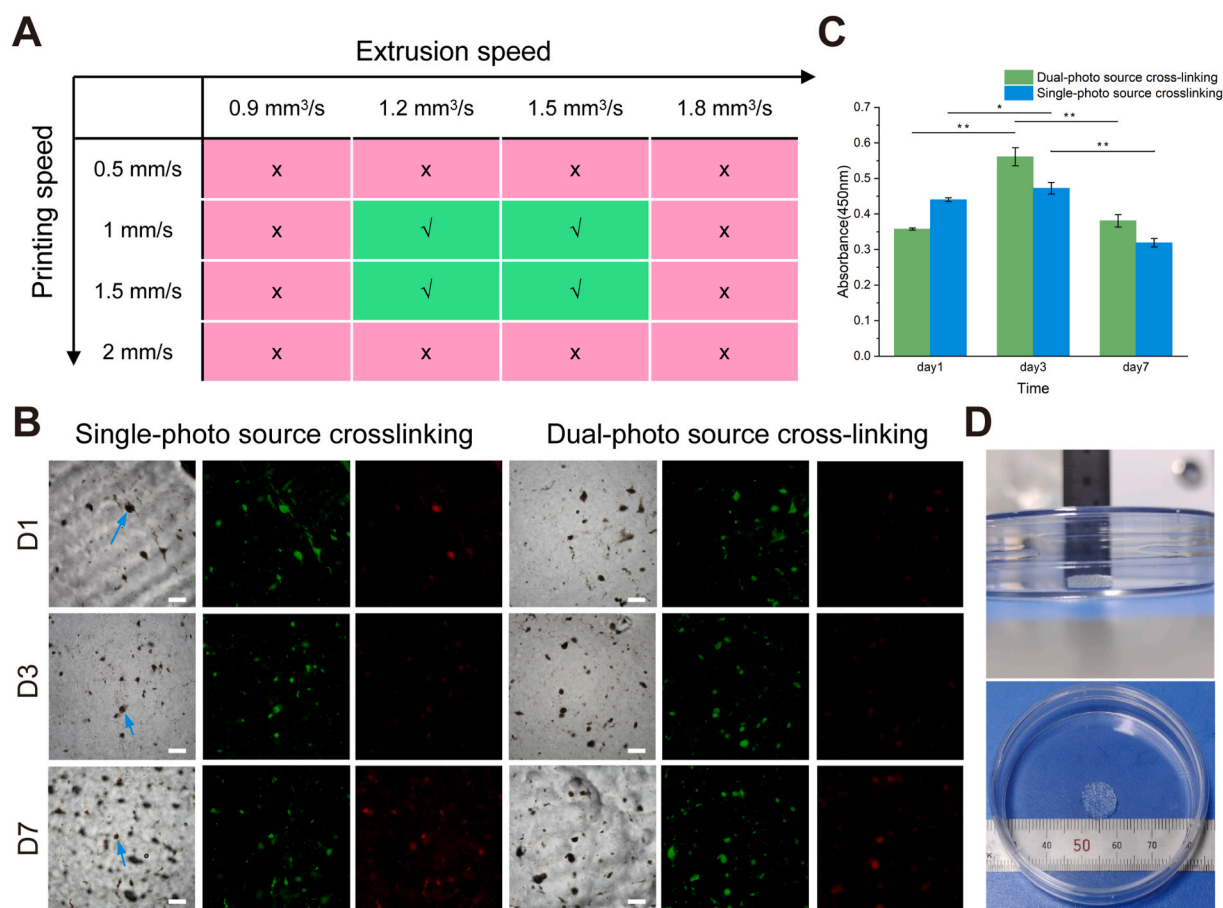
Fig. 4. Biocompatibility of cell spheres-laden hydrogel samples under different light strategies. (A) Different printing speeds and extrusion speeds affect the print quality of bioinks (B) Growth status of internal cells in single-photo source and dual-photo source sample groups, the arrows indicate cell spheres. Scale bar = 200 μm. (C) The CCK-8 results for cells inside hydrogels. (D) The morphology of the 3D bioprinted tissue containing skin organoids.

achieve complete cross-linking of the hydrogels. Both groups of cell sphere-laden hydrogel samples were cultured simultaneously for 7 days, and cell viability and proliferation assays were performed on days 1, 3, and 7, as shown in Fig. 4B and C. On the first day, a small number of cells died in both groups. On the third day, there was a small increase in the number of dead cells, but most cells remained viable. By the seventh day, the number of dead cells increased in both groups. The number of cell deaths was higher in the samples crosslinked with a single-photo source compared to those crosslinked with a dual-photo source. The CCK-8 results showed that the absorbance increased and then decreased with increasing incubation time, and the absorbance of the sample group crosslinked with a dual-photo source increased faster and decreased slower. These results proved that dual-photo source cross-linking is a suitable strategy.

According to the above printing parameters and lighting strategy, the morphology of the 3D bioprinted tissue containing skin organoids is shown in Fig. 4D. The three-dimensional structure is uniform, and the appearance is clear.

3.3. 3D bioprinting skin organoid accelerates wound closure

To evaluate the therapeutic efficacy of 3D bioprinted skin organoids, we utilized a nude mouse model of full-thickness skin wounds, as depicted in Fig. 5A. A 1 cm diameter wound was created on the back of each mouse, and three printed hydrogels with different ingredients were transplanted, with the printed hydrogel strictly adhered to the host on day 0. During the following observation period, the wounds were observed and photographed every 4 days. In the early stage of wound

healing, there was slight exudation on the surface, but the organoid group had integrated well with the host, and there was no significant inflammatory reaction at the wound margin during the observation interval.

As shown in Fig. 5B and C, the skin of nude mice gradually closed, the wound area gradually decreased, and the scabs fell off until approximately day 12. The rate of wound closure in the printed organoid group was significantly accelerated compared to all other groups, with a greater rate of re-epithelialization. The process of re-epithelialization refers to the migration and crawling of epidermal cells from the trauma tissue until they cover the entire trauma, restoring the protective barrier function of the epidermis. Fig. 5C presents the wound healing of the three groups of nude mice using a visualization method, through the detailed outline and integration of the region of interest (ROI). This facilitated intuitive analysis of the closure profiles of the full-thickness skin defects in the mice, showing that the mice in the printed organoid group had the smallest wound area and the best healing effect by the last day of the observation period. There were no significant differences in ROI area and wound healing rate between the groups before day 8, as shown by the statistical data in Fig. 5D and E. However, at days 12 and 16, significant improvement in wound closure could be observed in the printed organoid group compared to the Gel group and Gel + Susp group, with 93.76 % vs. 76.06 % vs. 75.26 % of the original wound area at day 16.

The 3D bioprinted skin organoid filled the defective skin and accelerated the epithelialization process of the wound, promoting faster wound healing. This demonstrates that the therapeutic effect of the 3D bioprinted skin organoid on wound healing was superior to that of pure
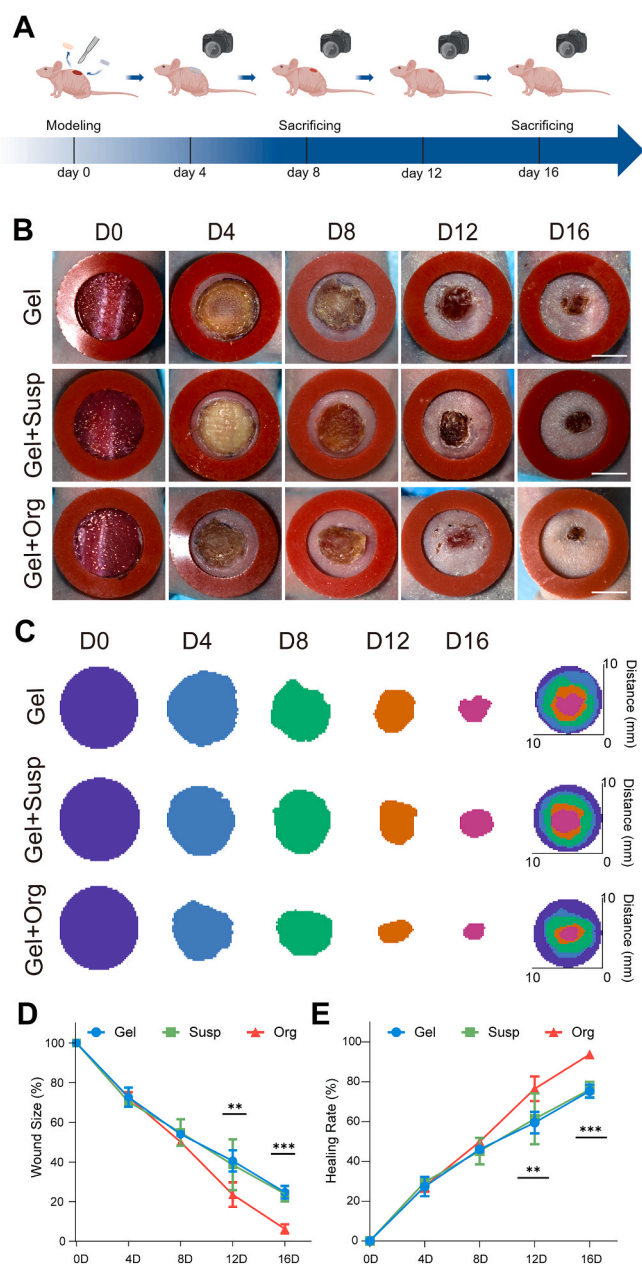
Fig. 5. The therapeutic effect observation of 3D bioprinting skin organoid in promoting the closure of skin defects in immunodeficiency mice. (A) The general observation of wound was photted by digital camera in every 4 days. (B) Representative photographs of the acute wound treated with different dressing. The red rubber ring was an anti-shrinkage ring with an inner diameter of 1 cm. With the duration of treatment, the wounds of all three groups tended to heal, and the printed organoid group showed the best rate of wound healing. Scale bar = 500 mm. (C) Simulation plots of wound closure. (D) The quantitative analysis of wound closure, (E) wound length of the wound sections in day 0, 4, 8, 12, 16. n = 6. At the same time point, the printed organoid group of mice had the smallest area of non-healing wounds, showing statistical differences in comparison with the remaining two groups at day 12 and 16. Statistical significances were analyzed using t-test and one-way ANOVA. *P < 0.05, **p < 0.01, ***p < 0.001 compared with control group.

hydrogels and cell suspensions.

3.4. 3D bioprinting skin organoid could improve wound healing quality and promote in-situ healing

Wound repair constitutes a meticulously orchestrated cascade,

encompassing distinct phases: hemostasis, inflammation, proliferation, and remodeling. To evaluate the therapeutic impact of the different treatments on wound healing progression, H&E staining was employed on biopsy specimens obtained on post-treatment days 8 and 16 from the Gel, Gel + Susp, and printed organoid groups. This histological analysis was performed to assess the status of epidermal integrity, the degree of epidermal and dermal apposition, as well as the extent of inflammatory cell infiltration within the wound sites (Fig. 6B). Extensive literature supports that during the inflammatory phase, there is a surge in inflammatory cell recruitment, which is succeeded by the proliferative phase, marked by neo-angiogenesis, fibroblast proliferation, and the advancement of re-epithelialization. The wound section in the gel group had many inflammatory cells aggregated in the dermis on day 8, meanwhile, it could be observed that the cells in the epidermis under the hydrogel were disorganized and the dermis was loosely connected to the epidermis with vacuolated structures, and the cells did not entirely feed into the wound, which had not yet healed completely. On the other hand, mice in the printed organoid group presented a thinner wound with a tighter structure, well-arranged cells in the epidermis, fewer inflammatory cells, and abundant vascularization and many erythrocytes, which were expected to facilitate the continuous proliferation of fibroblasts and the growth of granulation tissues to fill in the defective skin tissues. The epidermis of the printed organoid group was complete and well adhered to the dermis at 16 days after modeling, and the crista structure had developed, with a morphology closer to that of normal skin. Though the epidermis of the Gel + Susp group was structurally intact, and the dermal granulation tissue proliferation was obvious, while the epidermis of the Gel group was not completely healed, and the epidermis was obviously separated from the dermis. Meanwhile, the range of new tissue in the printed organoid group was significantly superior to that in the Gel group and Gel + Susp group, and the tissue morphology was closer to that of normal mouse skin, the dermal thickness was close to that of normal mouse skin at the margin of the wound, and the sebaceous glands and hair follicles like constructures in the epidermal layer was significantly more obvious compared with that in the other two groups, which indicated that skin organoids might accelerate skin appendages regeneration (Fig. 6B). There is a conclusion that 3D bioprinting skin organoid can promote re-epithelialization of wounds with tight epidermal dermal apposition, less inflammatory cell infiltration of wounds, and newly generated skin that more closely resembles normal skin structure.

Besides, collagen deposition is a key factor that determines skin strength and maturation. Masson staining results showed that the dermis of all three groups of wounds were formed by collagen fiber structure, mainly concentrated in the dermis, with a blue mesh structure. However, compared with Gel group, which demonstrated loose and thin dermal collagen fibers, Gel + susp and Gel + Org group presented aligned collagen fibers. (Fig. 6C). This result suggests that 3D bioprinting skin organoid promote wound collagen alignment, increase the neatness of collagen arrangement, and enhance the quality of wound healing.

Type I and III collagen is the main component of dermis, as the structural scaffold of extracellular matrix, it facilitates cell adhesion, chemotaxis and migration, whose structure and arrangement reveal the quality of wound healing. In addition, Type III collagen was associated with the generation of scar tissue. Therefore, the wounds condition of all groups was evaluated by analyzing Col-I and Clo-III immunohistochemical staining of the wound tissues on the 16th day, including the expression of collagen type I and collagen type III as well as the arrangement and distribution of collagen. These results demonstrated that type I collagen and type III collagen were expressed in all three groups, but type I collagen was expressed maximally while type III collagen was expressed minimally in the printed organoid group (Fig. 6F and G), compared to the other two groups and the arrangement of type I collagen and type III collagen was much more aligned in printed organoid group, while the remaining two groups were more distorted in
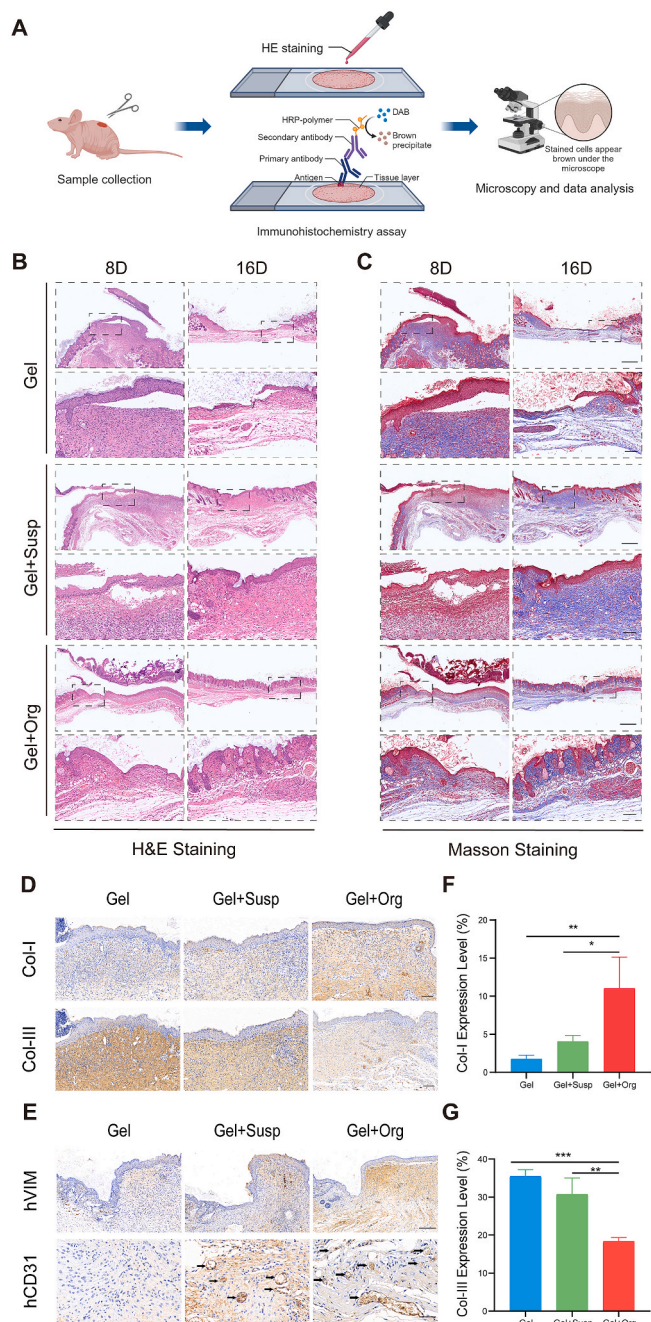
Fig. 6. 3D bioprinting skin organoid repairs and improves quality of wound healing through in-situ replacement. (A) The histopathological staining were proceeded to evaluate the quality of wound-healing. (B) H&E staining of the wound indicated the healing condition at 8 and 16 days. (C) Masson's staining of the wound sections at day 8 and day 16. Scale bar = 500 μm(Top). Scale bar = 100 μm(Bottom). (D) Immunohistochemical images of wound tissues stained by Col-I and Col-III (brown) on days 16, respectively. Scale bar = 100 μm. (E) Immunohistochemical images of wound tissues stained by human specific VIM and CD31 (brown) on days 16, respectively. Scale bar = 200 μm(Top). Scale bar = 50 μm(Bottom). (F) The quantitative analysis of Col-I, (G) Col-III of the wound sections in day 16. n = 3. Statistical significances were analyzed using *t*-test and one-way ANOVA. *P < 0.05, **p < 0.01, ***p < 0.001 compared with control group.

terms of collagen structure(Fig. 6D).

In order to verify the therapeutic effect of skin organoid constructed by human-derived cells on immunodeficient mice with large skin defects, Immunohistochemical staining with hVIM and hCD31 was employed to determine whether 3D bioprinting skin organoid could promote wound healing in situ. A clear observation reveals that, there is no expression of human-specific dermal marker VIM and CD31 at the edge of the wound in mice using hydrogel material alone, while abundant expression of hVIM and hCD31 was found in the suspension group and printed organoid group using cell therapy. Meanwhile the neo-vascularization was more abundant in printed organoid group, and the vascular density was significantly higher than the others (Fig. 6E), which is in accordance with the following results in Fig. 7B.

In summary, 3D bioprinting skin organoid can improve the quality of wound healing by integrally filling skin defects in situ, enhancing the compactness of epidermal cells and collagen arrangement of the dermis, as well as the overall tissue structure after application to large skin defects in mice, leading to skin repairs that tend to resemble normal skin, rather than scar tissue.

3.5. 3D bioprinting skin organoid promote re-epithelialization and vascularization

Re-epithelialization and vascularization are extremely important in the healing of skin defects [30]. Re-epithelialization involves migration, proliferation and differentiation of keratinocytes, and the process of epithelialization covers and closes the wound site and restores the skin barrier function [31]. Fig. 7A depicted experimental animals were undergone euthanasia and samples were taken from wound sites at day16. The process of vascularization involves the proliferation and migration of endothelial cells, and the neovascular network provides energy and nutrients to the wound tissue to promote wound healing. Immunofluorescence staining of CD31 was used to detect angiogenesis in the wound sections and quantitative immunofluorescence analysis was used to calculate neovascular density to assess the vascularization of skin wounds. As expected, neo-vessels as labeled by the CD31 (red) were found in the wounds of all three groups but compared with the cell Gel + Susp group and the Gel group, the CD31 expression was maximum in the printed organoid group, followed by the Gel + Susp group. Thus, the results of immunofluorescence quantitative analysis of vascular density showed that the vascular density of the printed organoid group was significantly higher than that of the remaining two groups, P < 0.01 (Fig. 7B and C). It is demonstrated that 3D bioprinting skin organoid can promote neovascularization of skin wounds with higher vascular density, which implied that the adequate blood supply was conducive to neoplastic skin growth and repair.

In Fig. 7E, immunofluorescence staining of K14 demonstrates epidermal thickness and re-epithelialization during wound healing after being modeled for 16 days. As an epidermal stem cell marker with proliferation and division ability in the basal layer of the epidermis, the expression of K14 in the traumatic epidermis of mice in the printed organoid group was higher and concentrated in the basal layer, whereas the expression of K14 in mice in the Gel group and the Gel + Susp group was dispersed and uneven, and the fluorescence intensity was significantly lower than that in the printed organoid group. In addition, by analyzing the statistical data on epidermal thickness, the epidermal thickness of mice in the printed organoid group was significantly lower than that of the other two groups, as shown in Fig. 7D.

Collectively, all these results suggest that the pro-healing effect of the 3D bioprinting skin organoid was better, highlighting the importance role of epidermal reconstruction and neovascularization.

3.6. 3D bioprinting skin organoid accelerated wound healing through inflammation inhibition

Employing a rodent model with extensive cutaneous lesions have substantiated the efficacy of three-dimensional bioprinted skin organoids in expediting wound closure. Henceforth, elucidating the intricate biological mechanisms underlying this enhanced healing capacity becomes imperative. To delve deeper into the underlying mechanisms, we
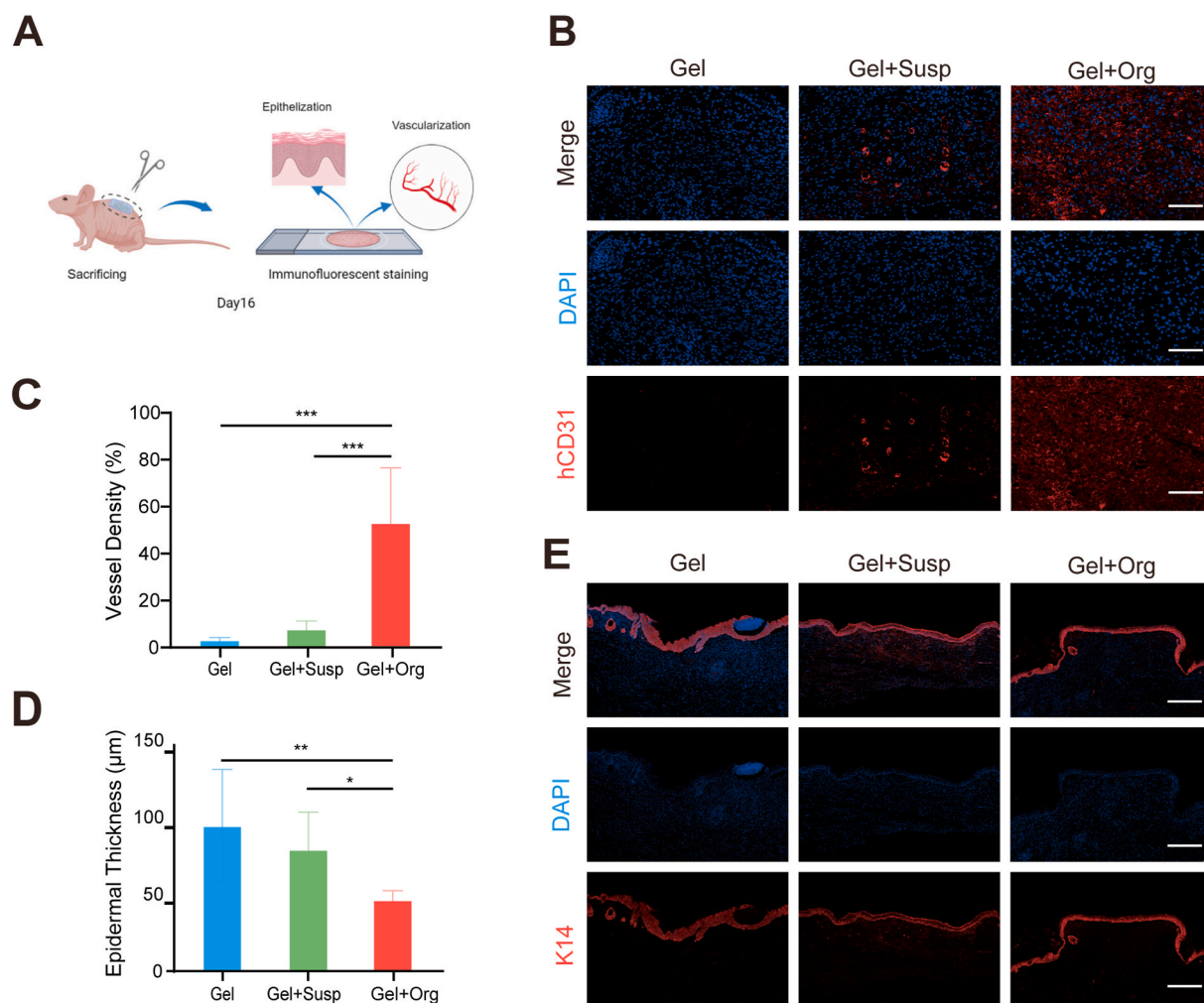
Fig. 7. 3D bioprinting skin organoid generate a tightly packed neoepidermal layer with more neovascularization. (A) Samples were taken at day16, and Immunofluorescence staining was performed to test re-epithelialization and neovascularization. (B–E) Immunofluorescence staining of CD31(B) and K14(E) on day 16. CD31, red; CK14, red. Scale bar = 50 μm. Quantitative analysis of (C) CD31 and (D) K14. Data are presented as mean ± SD (n = 3). *P < 0.05, ***P < 0.001 compared with control group.

embarked upon a comprehensive transcriptomic dissection utilizing samples derived from the Gel, Gel + Susp, and printed organoid group. The results unveiled conspicuous disparities in gene expression profiles across the various groups, with printed organoid group exhibiting a significantly enriched landscape of differentially expressed genes. Specifically, the analyses revealed an upregulation of 478 transcripts and a downregulation of 204 transcripts, as graphically represented in the Venn diagram, volcano plots, and heatmap (Fig. 8A–C). These differentially expressed genes were further interrogated through the lens of the Gene Ontology (GO) database, encompassing domains of biological processes, cellular components, and molecular functions. As depicted in Fig. 8D, the genes of T cell receptor associated signal pathway and humoral immune response were downregulated in the printed organoid group, which is compared to Gel + Susp group. The findings suggest that, even in cases involving allogeneic cell transplantation, the utilization of 3D bioprinting skin organoid demonstrates enhanced efficacy in promoting wound healing, while concurrently reducing inflammatory response and maintaining a relatively stable state of the wound tissue. Additionally, The 3D bioprinted skin organoids augmented the transcriptional activity of genes integral to the positive regulation of sarcolemma integrity and muscle contractility, thereby facilitating the acceleration of wound closure. (Fig. 8E). Moreover, an enhancement in the expression levels of genes pivotal to collagen biosynthesis and the activities of modifying enzymes was observed, suggesting a robust

extracellular matrix (ECM) remodeling and regenerative response (Fig. 8H). Furthermore, to elucidate the potential regulatory cascades governing these transcriptional alterations, we delved into pathway analysis utilizing the Kyoto Encyclopedia of Genes and Genomes (KEGG).The wound healing observed in the printed organoid group, as illustrated in Fig. 8F and G, demonstrated alterations in IL-17 signaling, NK cell-mediated cytotoxicity signaling, and cGMP-PKG signaling pathways that are closely associated with the regulation of inflammatory response. The collective findings of this study demonstrate that the 3D bioprinting skin organoid effectively expedite the process of wound healing by promoting pathways involved in skin regeneration and regulating proinflammatory response.

3.7. Discussion

In this study, we construct skin organoids by taking advantage of self-assembly potential of skin fibroblasts and keratinocytes together with endothelial cells. This spheroid-shaped skin organoid comprises surface-anchored keratinocytes surrounding a dermal core made of fibroblasts and endothelial cells, representing a micro-sized skin unit. We apply this unit to the treatment of full-thickness skin defects in immunodeficient mice, developing an unique sort of bio-ink which is optimal for spherical bioprinting, and employing extrusion-based 3D bioprinting and photo-crosslinking processes to construct biomaterials containing skin
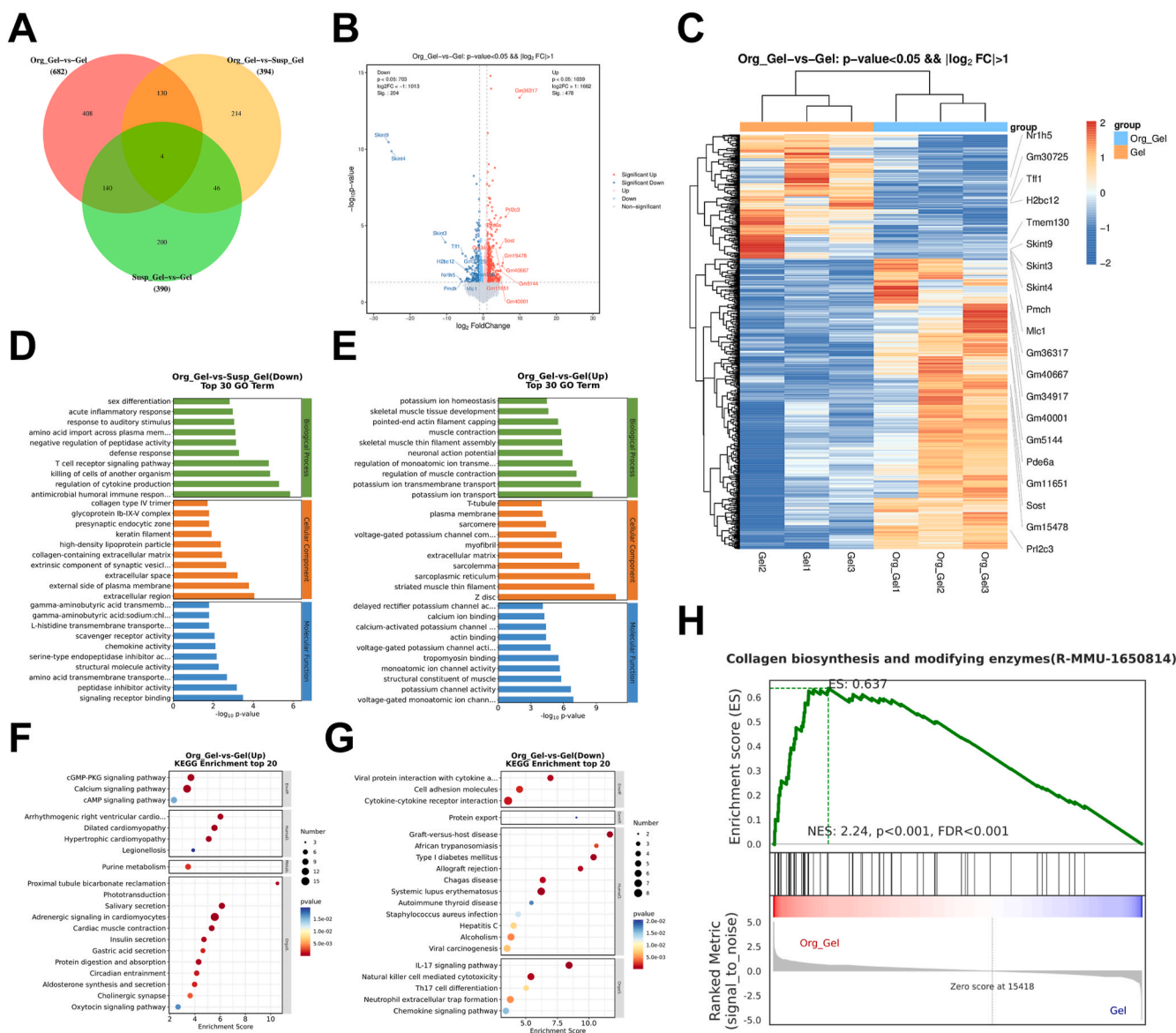
Fig. 8. Mechanistic analysis of wound healing with 3D bioprinting skin organoid treatment. (A) Venn diagram and (B)volcano plots of transcriptomic analysis of differentially expressed genes (n = 3 biologically independent samples). (C) Heatmap analysis of differentially expressed genes. (D) and (E) Portion of GO analysis of differentially up-regulated and down-regulated expressed genes among groups. (H) GSEA analysis of collagen biosynthesis between printed organoid group and Gel group. (F) and (G) Enriched KEGG pathways of printed organoid group versus Gel group. The size of the dots indicates the number of genes associated with indicated KEGG terms.

organoids that match the size and shape of the wound. The result turns out that this composite construct exhibits remarkable therapeutic efficacy of skin defects.

Current research on the treatment of skin defects mainly focuses on the development of biomaterials with special functions, such as anti-inflammatory and antibacterial biogels, or composite biomaterials loaded with skin cells or collagen [32,33]. These materials have played a certain role in promoting wound healing but still have obvious limitations. Due to the lack of components that can regenerate dermis and epidermis in situ, this leads to increased scarring and severe fibrosis of the newly formed skin, with its structure and function being significantly different from that of normal skin [34,35]. In this study, we found that Bioprinting 3D constructs embedded with skin organoids exhibited superior wound repair capabilities compared to simple biomaterials or those loaded with cell suspensions. Not only was the wound healing process the fastest, but more importantly, we detected human dermis and vascular structures in the mouse wound sites, which indicated that

3D bioprinting skin organoid might promote would in-situ regeneration in a relatively more normal way. This result indicates that skin organoids possess great potential and clinical application prospects for skin defect repair.

Skin organoids are a hot research field in recent years. Discussing their function involves indispensable in vivo experiments, which include how to better implant these organoids into animals. Currently, skin organoids are mostly implanted into animals by direct coverage, injection, or through small incisions [36–38]. These methods are simple and direct, generally suitable for small-scale implantation. However, for patients with large areas of skin defects, the aforementioned implantation methods are not convenient enough, and the hostile microenvironment of the wound could directly damage the implanted skin organoids [39]. Therefore, this study employed 3D bioprinting technology to address this issue. 3D bioprinting technology is an upgraded version of common 3D printing technology where the bio-ink mainly includes cell suspension and hydrogel [40–43]. As skin organoids are

three-dimensional cell spheroids, they present more complexity in size, structure, and function compared to two-dimensional cells, indicating they require more specific printing technology [44–47]. During our research, we prepared a unique bio-ink with embedded skin organoids and successfully combined extrusion bioprinting technology with dual-photo source cross-linking technology.

The extrusion bioprinting technology based on temperature field regulation prepares pre-crosslinked biological structures and completes the effective combination of skin organoids and hydrogels [48]. Subsequently, a dual -photo source cross-linking process was innovatively proposed [27]. Compared with the traditional single photo source or the common photo-curing bioprinting technology, the dual-photo source cross-linking can first reduce the illumination time on the premise of ensuring that the bioink is completely formed, thereby reducing the adverse effects of light radiation on the sphere skin organoids [49].In summary, extrusion bioprinting technology combined with dual-photo source cross-linking technology provides more options for wound repair methods. Finally, we obtained the 3D bioprinting skin organoid that match the shape and size of the wound. Not only was this biological structure conducive to the survival of skin organoids, but it also possessed water-absorption capabilities, effectively reducing early exudation from the wound. Moreover, the customized shape and size made it more convenient for implantation into the skin defect, presenting high clinical translational value.

In vivo experiments indicated that 3D bioprinting skin organoid transplantation significantly accelerated would healing rate, but also promoted the healing quality. The arrangement of collagen in normal skin tissue is very different from that in scar tissue, which indicates that the collagen arrangement shown in Masson staining images proved high healing quality by organoid transplantation. Furthermore, this study conducted a preliminary analysis of the mechanism of the therapeutic efficacy of the 3D bioprinting skin organoid to skin defect, which was not involved in previous studies. By RNA sequencing, we tested that skin organoids could reduce the expression of inflammation-related genes, involving cellular pathways such as IL-17, NK cells, and the cGMP-PKG pathway, providing the direction for further research on the mechanism of regulating inflammation during wound healing.

In summary, this study pioneers the combination of two cutting-edge technologies, skin organoid technology and 3D bioprinting technology to develop a composite construct embedded with skin organoids. It also screened out an optimum bio-ink and innovatively merged extrusion bioprinting technology with dual-photo source cross-linking technology to make sure skin organoids can perform better when embedded into hydrogel. The research verifies that the printed biological structures not only make it more convenient for implantation but also exhibit a robust therapeutic effect in promoting in situ wound healing. This demonstrates significant clinical translational value and give new insights to the treatment of large-area skin defects in the future. However, this study still has some limitations. First, the observation time for skin wound healing in mice in this study is short, and subsequent studies could extend the observation time to analyze the degree of tissue fibrosis after wound healing and detect the role of skin organoids in scar repair. In addition, this study focuses on discussing the therapeutic effects of skin organoids on wound repair, while only a superficial analysis of its repair mechanisms is conducted. Subsequent studies could focus more on exploring the mechanisms of skin organoids in regulating inflammation during wound healing.

4. Conclusion

In general, the current study demonstrates that self-assembly of keratinocytes, fibroblasts and endothelial cells can successfully generate sphere skin organoids. By utilizing extrusion bioprinting technology combined with dual-photo source cross-linking technology, we designed an 3D bioprinting skin organoid. When this 3D bioprinting skin organoid was applied to full-layer skin defects in immunodeficient mice the

therapeutic efficacy of wound was significantly enhanced. Remarkably, we verified that skin organoid could promote in-situ healing, facilitate epithelialization and vascularization and improve wound healing quality. We also preliminarily found that skin organoid could effectively expedite the process of wound healing by promoting pathways involved in regulating proinflammatory response, which provide new insights into the repair of large-area skin defects.

Ethics approval and consent to participate

CRediT authorship contribution statement

Tao Zhang: Writing – original draft, Investigation, Formal analysis, Data curation, Conceptualization. **Shihao Sheng:** Writing – original draft, Methodology, Investigation. **Weihuang Cai:** Methodology, Investigation, Data curation. **Huijian Yang:** Conceptualization, Formal analysis. **Jiameng Li:** Writing – original draft, Methodology, Investigation, Formal analysis, Data curation. **Luyu Niu:** Validation, Methodology, Investigation. **Wanzhuo Chen:** Validation, Methodology, Investigation. **Xiuyuan Zhang:** Validation, Investigation. **Qirong Zhou:** Validation, Supervision, Investigation. **Chuang Gao:** Conceptualization. **Zuhao Li:** Validation, Methodology. **Yuanwei Zhang:** Validation, Methodology. **Guangchao Wang:** Supervision, Methodology. **Hao Shen:** Supervision, Resources. **Hao Zhang:** Validation, Methodology. **Yan Hu:** Validation, Methodology. **Zhifeng Yin:** Writing – original draft, Methodology, Data curation. **Xiao Chen:** Writing – review & editing, Validation, Methodology, Investigation, Funding acquisition. **Yuanyuan Liu:** Writing – review & editing, Validation, Investigation, Funding acquisition, Formal analysis, Conceptualization. **Jin Cui:** Writing – review & editing, Validation, Methodology, Funding acquisition, Formal analysis, Conceptualization. **Jiacan Su:** Writing – review & editing, Resources, Project administration, Funding acquisition, Conceptualization.

Declaration of competing interest

The authors declare no conflict of interest.

Acknowledgments

Appendix A. Supplementary data

Supplementary data to this article can be found online at https://doi.org/10.1016/j.bioactmat.2024.08.036.

References

[1] H.E. Talbott, et al., Wound healing, fibroblast heterogeneity, and fibrosis, Cell Stem Cell 29 (8) (2022) 1161–1180.
[2] Y. Luo, et al., Autograft microskin combined with adipose-derived stem cell enhances wound healing in a full-thickness skin defect mouse model, Stem Cell Res. Ther. 10 (1) (2019) 279.

[3] C.C. Yates, P. Hebda, A. Wells, Skin wound healing and scarring: fetal wounds and regenerative restitution, Birth Defects Res C Embryo Today 96 (4) (2012) 325–333.

[4] T. Guan, et al., Self-assembling peptide-based hydrogels for wound tissue repair, Adv. Sci. 9 (10) (2022) e2104165.

[5] C. Lindholm, R. Searle, Wound management for the 21st century: combining effectiveness and efficiency, Int. Wound J. 13 (Suppl 2) (2016) 5–15. Suppl 2.

[6] C.K. Sen, Human wound and its burden: updated 2020 compendium of estimates, Adv. Wound Care 10 (5) (2021) 281–292.

[7] H.E. desJardins-Park, et al., From chronic wounds to scarring: the growing Health care burden of under- and over-healing wounds, Adv. Wound Care 11 (9) (2022) 496–510.

[8] Z. Yao, J. Niu, B. Cheng, Prevalence of chronic skin wounds and their risk factors in an inpatient hospital setting in northern China, Adv. Skin Wound Care 33 (9) (2020) 1–10.

[9] H.S. Kim, et al., Advanced drug delivery systems and artificial skin grafts for skin wound healing, Adv. Drug Deliv. Rev. 146 (2019) 209–239.

[10] J. Lee, et al., Hair-bearing human skin generated entirely from pluripotent stem cells, Nature 582 (7812) (2020) 399–404.

[11] X. Han, et al., Landscape of human organoids: ideal model in clinics and research, Innovation 5 (3) (2024) 100620.

[12] P. Ebner-Peking, et al., Self-assembly of differentiated progenitor cells facilitates spheroid human skin organoid formation and planar skin regeneration, Theranostics 11 (17) (2021) 8430–8447.

[13] Deng. Shunshu, et al., Harvest of functional mesenchymal stem cells derived from in vivo osteo-organoids, Biomater. Transl. 4 (4) (2023) 270–279.

[14] W. Zakrzewski, et al., Stem cells: past, present, and future, Stem Cell Res. Ther. 10 (1) (2019) 68.

[15] J. Dulak, et al., Adult stem cells: hopes and hypes of regenerative medicine, Acta Biochim. Pol. 62 (3) (2015) 329–337.

[16] Z. Tian, et al., Introduction to stem cells, Prog Mol Biol Transl Sci 199 (2023) 3–32.

[17] Xu. Yan, et al., Large scale, high purity, high quality isolation of mesenchymal stem cells from osteo-organoids, Biomater. Transl. 5 (1) (2024) 84–85.

[18] S. Kirchner, V. Lei, A.S. MacLeod, The cutaneous wound innate immunological microenvironment, Int. J. Mol. Sci. 21 (22) (2020).

[19] W.L. Ng, et al., Skin bioprinting: impending reality or fantasy? Trends Biotechnol. 34 (9) (2016) 689–699.

[20] M. Dey, I.T. Ozbolat, 3D bioprinting of cells, tissues and organs, Sci. Rep. 10 (1) (2020) 14023.

[21] M.S. Kang, et al., Advances and innovations of 3D bioprinting skin, Biomolecules 13 (1) (2022).

[22] Yu. Xingge, et al., Three-dimensional bioprinting biphasic multicellular living scaffold facilitates osteochondral defect regeneration, Interd. Mater. 6 (2) (2024) 1–19.

[23] M. Askari, et al., Recent progress in extrusion 3D bioprinting of hydrogel biomaterials for tissue regeneration: a comprehensive review with focus on advanced fabrication techniques, Biomater. Sci. 9 (3) (2021) 535–573.

[24] L. Ning, X. Chen, A brief review of extrusion-based tissue scaffold bio-printing, Biotechnol. J. 12 (8) (2017).

[25] Zheng. Ke, et al., Recent progress of 3D printed vascularized tissues and organs, Smart Mater. Med. 6 (5) (2024) 183–195.

[26] L.Y. Daikuara, et al., In vitro characterisation of 3D printed platelet lysate-based bioink for potential application in skin tissue engineering, Acta Biomater. 123 (2021) 286–297.

[27] T.J. Tigner, et al., Comparison of photo cross linkable gelatin derivatives and initiators for three-dimensional extrusion bioprinting, Biomacromolecules 21 (2) (2020) 454–463.

[28] R.H. Jin, et al., Three-dimensional bioprinting of a full-thickness functional skin model using acellular dermal matrix and gelatin methacrylamide bioink, Acta Biomater. 131 (2021) 248–261.

[29] X. Zhao, et al., Photocrosslinkable gelatin hydrogel for epidermal tissue engineering, Adv. Healthcare Mater. 5 (1) (2016) 108–118.

[30] A. Das, et al., Oncostatin M improves cutaneous wound Re-epithelialization and is deficient under diabetic conditions, J. Invest. Dermatol. 142 (3 Pt A) (2022) 679–691.e3.

[31] K. Chen, et al., Hyaluronic acid-modified and verteporfin-loaded polylactic acid nanogels promote scarless wound healing by accelerating wound re-epithelialization and controlling scar formation, J Nanobiotechnology 21 (1) (2023) 241.

[32] C. Huang, et al., Anti-inflammatory hydrogel dressings and skin wound healing, Clin. Transl. Med. 12 (11) (2022) e1094.

[33] H. Cheng, et al., Sprayable hydrogel dressing accelerates wound healing with combined reactive oxygen species-scavenging and antibacterial abilities, Acta Biomater. 124 (2021) 219–232.

[34] C. Dai, S. Shih, A. Khachemoune, Skin substitutes for acute and chronic wound healing: an updated review, J. Dermatol. Treat. 31 (6) (2020) 639–648.

[35] M. Monavarian, et al., Regenerative scar-free skin wound healing, Tissue Eng., Part B 25 (4) (2019) 294–311.

[36] J. Diao, et al., Sweat gland organoids contribute to cutaneous wound healing and sweat gland regeneration, Cell Death Dis. 10 (3) (2019) 238.

[37] J. Ma, et al., Application of an iPSC-derived organoid model for localized scleroderma therapy, Adv. Sci. 9 (16) (2022) e2106075.

[38] X. Sun, et al., Sweat gland organoids originating from reprogrammed epidermal keratinocytes functionally recapitulated damaged skin, Adv. Sci. 8 (22) (2021) e2103079.

[39] J.P. Junker, E.J. Caterson, E. Eriksson, The microenvironment of wound healing, J. Craniofac. Surg. 24 (1) (2013) 12–16.

[40] D. Banerjee, et al., Strategies for 3D bioprinting of spheroids: a comprehensive review, Biomaterials 291 (2022) 121881.

[41] C. Mandrycky, et al., 3D bioprinting for engineering complex tissues, Biotechnol. Adv. 34 (4) (2016) 422–434.

[42] K. Hölzl, et al., Bioink properties before, during and after 3D bioprinting, Biofabrication 8 (3) (2016) 032002.

[43] Yu. Xingge, et al., Osteoimmunomodulatory bioinks for 3D bioprinting achieve complete regeneration of critical-sized bone defects, Compos. Part B-Eng. 3 (1) (2024) 111256.

[44] Y. Kim, J.H. Ju, Generation of 3D skin organoid from cord blood-derived induced pluripotent stem cells, J. Vis. Exp. 146 (2019).

[45] D. Dutta, I. Heo, H. Clevers, Disease modeling in stem cell-derived 3D organoid systems, Trends Mol. Med. 23 (5) (2017) 393–410.

[46] G. Rossi, A. Manfrin, M.P. Lutolf, Progress and potential in organoid research, Nat. Rev. Genet. 19 (11) (2018) 671–687.

[47] F. Wang, et al., Organoid bioinks: construction and application, Biofabrication 16 (3) (2024).

[48] I.T. Ozbolat, M. Hospodiuk, Current advances and future perspectives in extrusion-based bioprinting, Biomaterials 76 (2016) 321–343.

[49] Y. Song, et al., Dual growth factor delivery using photo-cross-linkable gelatin hydrogels for effectively reinforced regeneration of the rotator cuff tendon, ACS Appl. Bio Mater. 7 (2) (2024) 1146–1157.